This document is the Accepted Manuscript version of a Published Work that appeared in final form in **Applied Materials Interfaces**, peer review and technical editing by the publisher. To access the final edited and published work see: https://onlinelibrary.wiley.com/doi/abs/10.1002/admi.201500855; DOI: 10.1002/admi.201500855

An Organic Spin Valve Embedding a Self-Assembled Monolayer of Organic Radicals

*Lorenzo Poggini, Giuseppe Cucinotta, Abdul-Muizz Pradipto, Marco Scarrozza, Paolo Barone, Andrea Caneschi, Patrizio Graziosi, Marco Calbucci, Raimondo Cecchini, Valentin Alek Dediu, Silvia Picozzi, Matteo Mannini, * and Roberta Sessoli **

Dr. L. Poggini, Dr. G. Cucinotta, Prof. A. Caneschi,
Dr. M. Mannini, Prof. R. Sessoli
Dipartimento di Chimica "U. Schiff" and INSTM
UdR Firenze
Università di Firenze
Via della Lastruccia 3-13, 50019 Sesto Fiorentino , Italy
E-mail: matteo.mannini@unifi .it;
roberta.sessoli@unifi .it

Dr. A.-M. Pradipto, Dr. M. Scarrozza, Dr. S. Picozzi
Consiglio Nazionale delle Ricerche
CNR-SPIN Chieti
Via dei Vestini, 31, 66100 Chieti , Italy

Dr. P. Barone
Consiglio Nazionale delle Ricerche
CNR-SPIN L'Aquila
Via Vetoio, 10, 67100 Coppito L'Aquila , Italy

Dr. P. Graziosi, Dr. M. Calbucci, Dr. V. A. Dediu
Consiglio Nazionale delle Ricerche – Istituto per lo Studio
dei Materiali Nanostrutturati ISMN-CNR
Via Piero Gobetti 101, 40129 Bologna , Italy

Dr. R. Cecchini
Laboratorio MDM
IMM-CNR
Unità di Agrate Brianza
Via C. Olivetti 2, 20864 Agrate Brianza , (MB) , Italy

A novel functionalization of a ferromagnetic electrode employed in spintronic devices is reported. Self-assembling monolayer technique has been used to chemisorb a paramagnetic phosphonate functionalized nitronyl-nitroxide radical (NitPO) on the ferromagnetic $La_{0.7}Sr_{0.3}MnO_3$ (LSMO) manganite surface. This interfacial layer causes clearly detectable modifi cations of the behavior in prototypical LSMO/NitPO/Gaq_3 /AlO_x /Co vertical spintronic devices at temperatures below the ferromagnetic alignment (estimated by density functional theory) of the magnetic moments of NitPO and LSMO. This behavior can be justified by a significant spin filtering effect at the engineered interface, with a carrier selection (spin-up) opposite to that of the LSMO/Gaq_3 interface (spin-down). It is proposed that the engineering of spin injecting interfaces with molecules having magnetic moment enables additional mechanisms to control and manipulate the spin polarization of currents in spintronic devices.

1. Introduction

Molecular magnetism is a very fertile fi eld of nanoscience, due to the intriguing properties of single molecule magnets merging classical and quantum behavior in a nanosized object. [1–4] From the applicative point of view, the use of magnetic molecules in spintronics can offer several advantages due to different aspects. On one side, molecular magnets have the functionality of carrying magnetic information down to the molecular size.

This encourages the race toward miniaturization of magnetic devices as well as the exploitation of magnetic molecules for quantum computing, [5] although this solution is still hindered by the low working temperature. [6–8] On the other side, nonmagnetic molecular materials like organic semiconductors (OSCs) have been considered rather extensively during the past decade in the search for optimal combinations for prototypical devices in the area of spintronics technology, i.e., spin-valves. [9] The magnetoresistance in such devices, which consist of ferromagnetic metal electrodes sandwiching a semiconducting material, depends on the injection and transport of the spin through the semiconductor spacer.

OSCs typically possess weak spin-orbit coupling and, because of this, they guarantee longer spin coherence time compared to both inorganic semiconductors and metals. In this context, different organic materials, such as pentacene [10] and *tris* (8 hydroxyquinoline) aluminium(III) (Alq_3) [11,12] and the gallium(III) analogue (Gaq_3), [13] have been employed in combination with several ferromagnetic metals, such as Fe and Co:TiO_2 [10] or Co and $La_{0.7}Sr_{0.3}MnO_3$ (briefly termed LSMO). [11,12] The changes of physical properties of both the metal and organic molecule at the interface have also attracted great scientific interests, so that the ad hoc term spinterface [14,15] has been advanced to describe the topic. From the organic side the spinterface describes the spin filtering effects caused by the spin-dependent hybridization of the organic and metallic orbitals, leading to different interfacial broadening (and hence transmissivity) of the localized organic states for the two spin channels. [14] On the other hand, it has been shown both experimentally [16] and theoretically [17–19] that some organic molecules can affect the magnetic properties of the underlying magnetic surface, in terms of magnitude and direction of magnetic moments and spin polarization as well as of strength of exchange interactions. Moreover, coupling between the spins of transition-metal based molecular magnets and magnetic surfaces can be obtained promoting surface-induced magnetic ordering of the molecular layer [20] and the possibility to switch the molecular spin orientation by switching the spin orientation of the surface. [21] These works have opened the path for controlling the magnetic properties of the surface of the electrodes. The modification of the spinterface by inserting a molecular layer is strongly supported by the richness of chemical systems that can be chemisorbed onto the spin-injecting electrode surface and the use of wet chemistry can widen significantly the technological playground. For instance, the possibility to tune the properties of the LSMO substrate and its spin-injection properties by grafting to the surface ad hoc functionalized alkyl chains through a chemisorption, i.e., the self-assembly of a monolayer (SAM) from solution, has been recently explored. The insertion of the alkyl phosphonic unit as passivating layer on the LSMO has been found to be compatible with the observation of a spin-valve effect in a nanoindented device, [22] a relevant insight that can be correlated for instance with the fact that similar molecular layer reduces charge trapping problems in OSC-based fi eld emission transistors. [23] Following these encouraging results, it is appealing to investigate the effect of a layer of paramagnetic centres, [24–26] such as organic magnetic molecule, i.e., radical units, such as thiazyl, [27] verdazyl, [28] and nitroxides, [29] on

the spin-injection and spin filtering phenomenon at organic spintronic interfaces. First, this research should help revealing the possible drawbacks of the presence of paramagnetic centres for the propagation of the spin polarization following an approach widely used to study the spin scattering processes in inorganic spintronics. [30] On the other hand, the coupling between the spins of paramagnetic molecules or molecular magnets and magnetic electrodes could allow the control of the spin injection.

In this work, a stable nitronyl-nitroxide radical (NNR) functionalized with a protected phosphonate group has been synthesized and a monolayer of these radicals was assembled on LSMO and chemically characterized using specific surface sensitive tools. A detailed theoretical investigation based on density functional theory (DFT) of the adsorption process as well as of the resulting electronic structure, confirmed that the radical nature of the organic molecules is retained and suggests that a weak ferromagnetic interaction with the magnetic LSMO substrate is present at low temperature. A vertical spin valve embedding a monolayer of radicals between the LSMO electrode and Gaq_3 was found to follow the typical magnetoresistance

trend of such vertical devices although clearly detectable differences of magnetoresistance and electrode switching fields were observed roughly in the same temperature range where interaction between the molecular layer and the manganite, according to DFT calculations, becomes relevant.

2. Synthesis and Characterization of the Radical

The functionalized NNR system (2-(diethyl 4-methylbenzylphosphonate)-4,4,5,5-tetramethylimidazoline- 1-oxyl-3-oxide, abbreviated in $NitPOR_2$ hereafter, was synthetized by following the procedure described in **Figure 1** using the Arbuzov reaction [31] to obtain the diethyl 4-formylbenzylphosphonate in accordance with literature procedures. [32] Then, adopting the usual steps of condensation of this aldehyde with 2,3-di(hydroxyamino)-2,3-dimethylbutane [21] and subsequent oxidation of the 4,4,5,5-tetramethyl-imidazolidine- 1,3-diol derivative, [33] the functionalized $NitPOR_2$ system was obtained after a purification on silica gel column (eluted with $CH_2 Cl_2$ /MeOH, 3/1). The bulk phase of this compound was characterized by using mass spectrometry, IR spectrometry, and electron paramagnetic resonance (see Figures S1 and S2 in the Supporting Information). In particular mass spectra analysis indicated the presence of the molecular peak at 383.11 *m/z* with the expected isotopic distribution structure; additionally it was also possible to identify typical fragmentation peaks of NNR systems: [24] 391.18 *m/z* $[M O+H+Na]^+$, 369.18 *m/z* $[M O+2H]^+$, 353.18 *m/z* $[M-2O+2H]^+$, 281.14 *m/z* $[M-2Et-3O+4H]^+$. The Fourier transform infrared (FT-IR) spectrum (see Figure S2a in the Supporting Information) presents fingerprint bands of the phosphonate group at 1231 cm^{-1} ascribable to the stretching (P O), 1167 cm^{-1} attributed to the stretching (C P) and 900–1050 cm^{-1} coming from the stretching (P OR), plus the N O stretching at 1393 cm^{-1} confirming the coexistence of the nitronyl-nitroxide radical function and of the phosphonate linker group. The recorded Electron Paramagnetic Resonance (EPR) spectrum (see Figure S2b in the Supporting Information) of a 1×10^{-3} M solution in dichloromethane of NitPOR 2 was in line with what expected for a nitronyl-nitroxide function showing the typical five lines structure centered around $g = 2.009$ with a relative intensity of 1:2:3:2:1 originated by two equivalent nitrogen nuclei 14 N ($I = 1$) with an approximate hyperfine coupling of 7.5 G. [29,34]

3. Preparation and Characterization of the NitPO Monolayer

By using a standard self-assembling strategy [24,35] (see the Experimental Section), a monolayer of NitPO molecules (where the acronym indicates that the monolayer is formed with the loss of the two ethyl groups, *R*) was assembled from solution (see Figure 1) on a 15 nm LSMO film prepared by channel spark ablation according to earlier reports, [36] deposited on NGO ($NdGaO_3$). The functionalized LSMO substrate was characterized by X-ray photoelectron spectroscopy (XPS) and time-of-flight secondary ion mass spectrometry (ToF-SIMS), see **Figure 2**. A clearly visible N1s peak, absent in the pristine substrate, centered at 399.3 eV can be directly ascribable to a NNR functional group, indicating the successful deposition of molecules on surface (Figure 2 a). [37,38] The XPS analysis of a bulk NitPOR2 sample features in fact an N1s peak centered at 399.2 eV, in agreement with literature data. [39,40] For the deconvolution of the N1s peak was necessary to use three components due to an X-ray induced damage in line with similar behavior of the bulk sample (see Figure S2c in the Supporting Information). We notice that the grafting process cannot be followed by monitoring the presence of the phosphorous on the surface (in the bulk at 132.9 eV) [37,38] because of the overlap of the P2p peak with Sr3d signal of the substrate. In order to confirm the grafting of the NitPO system (i.e., the formation of a chemical bond between the molecule and the substrate) ToF-SIMS characterization was carried out. A comparison between the ToF-SIMS spectra acquired on the monolayer deposit and on the massive phase is reported in Figure 2 b. Actually, in the 270–410 *m/z* region, it is evident that the [M] + peak of NitPOR 2 found at 383.11 *m/z* in the bulk is absent in the monolayer sample while a signal centered at 331.18 *m/z* is present only in the SAM sample indicating that a new species is formed on surface due to the deposition process. Indeed this distribution comes from a [M 2Et+4H] + ion and corresponds to a fragment of the NitPO without the two ethyl groups thus confirming the occurrence of an hydrolysis reaction and the formation of a phosphonic function that can be chemisorbed at the manganite surface. Moreover, the formation of a chemical bond between the phosphonic function and the LSMO surface is supported by the inspection of ToF-SIMS spectra in the region from 253 to 261 *m/z* (see Figure S3 in the Supporting Information): only in the monolayer a molecular fragment at 259 *m/z* is present. This corresponds to a molecular fragment (without the two ethyl groups of phosphonate linker) directly bound to a strontium atom and agrees with Sr-enriched termination of LSMO evidenced in our previous investigations. [41]

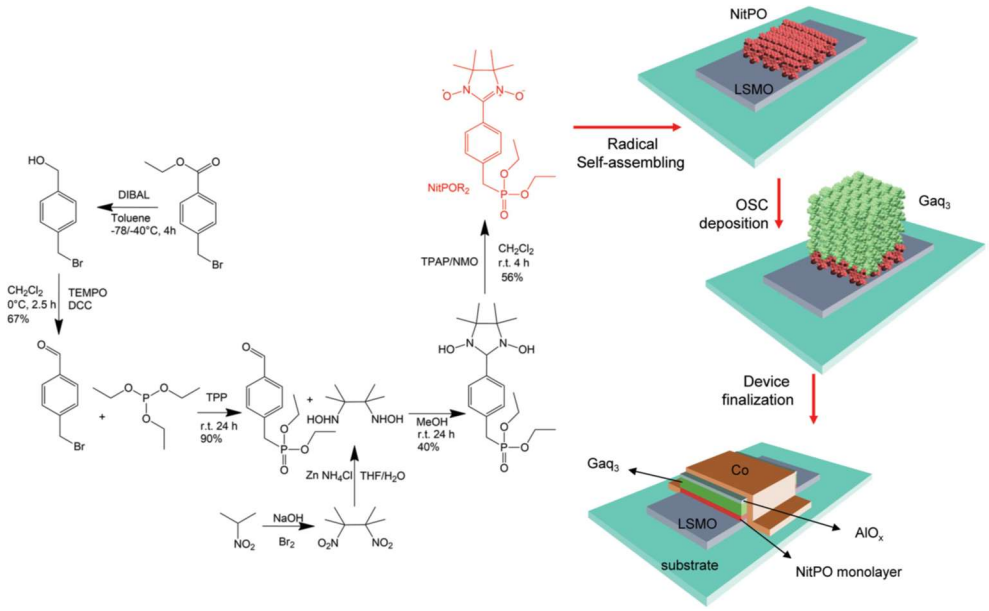

Figure 1. Schematic description of the synthesis of the radical (2-(diethyl 4-methylbenzylphosphonate)-4,4,5,5-tetramethylimidazoline-1-oxyl-3-oxide, $NitPOR_2$, their chemisorption on the LSMO electrode, and the realization of the organic vertical spin valve LSMO/NitPO/Gaq_3 /AlO_x /Co.

4. Ab Initio Modeling

4.1. Adsorption Geometry and Energetics

Although there are consistent evidences that the NitPO molecules are chemically grafted to the LSMO, it is not straightforward to assess if the radical character is maintained. In particular, the presence of the magnetic substrate does not allow to employ EPR spectroscopy and the detection of magnetism through synchrotron radiation is extremely challenging for light elements like O and N. In order to have insights from modeling, fi rst principles calculations based on DFT have been performed to simulate the adsorption of nitronyl-nitroxide phosphonate organic radical on the LSMO magnetic surface. We used the NitPO radical as absorbing molecule on the surface, as indicated by the ToF-SIMS characterization (see Figure S4 and computational details in the Supporting Information) and we simulated different adsorption sites in order to evaluate the most stable optimized structures of NitPO/LSMO interfaces (**Figure 3**). The adsorption energy has been estimated by subtracting from the total energy of the relaxed NitPO/LSMO interface, the total energies of the isolated subsystems, i.e., the NitPO molecule in vacuum and the LSMO slab for the clean surface (with the respective termination layers, MnO_2 and LaSrO, Equation (1)), i.e.

$$E_{ads} = E_{NitPO/LSMO} - E_{NitPO} - E_{LSMO} \quad (1)$$

As such, a negative E_{ads} implies that the adsorption is energetically favoured. For NitPO/MnO_2 and NitPO/LaSrO interfaces, the adsorption energies were estimated as -2.08 and -4.68 eV, respectively, indicating that the adsorption of NitPO radical on the LSMO surface is energetically favorable, regardless of the layer termination, with a stronger bonding to the LaSrO surface. All other considered starting configurations featured smaller magnitudes of the adsorption energy (i.e., leading to a less stable configuration) and are therefore not further discussed. Compared to the isolated system, some differences in the adsorbed structure of the molecule are rather clearly visible, in particular related to the structural coordination of the phosphonate group attached to the surface (see Figure 3 and discussion in the Supporting Information). Of particular relevance is that in the most stable structural configurations (for both termination layers) the spins of the radical and LSMO surface are ferromagnetically (FM) aligned. Geometry relaxations with antiferromagnetic (AFM) alignment result in similar structures, their total energies being slightly higher when compared to FM values. Using the FM relaxed structures, the total energy differences between FM and AFM alignments result in very small values (namely ΔE_{FM-AF} = -1.3 and -0.6 meV for NitPO/MnO_2 and NitPO/LaSrO, respectively). This points to a weak magnetic interaction between the radical and the oxide surface, with any consequence driven by the magnetic coupling expected to manifest only at very low temperatures (see below) corresponding to an approximate range between 85 and 40 K.

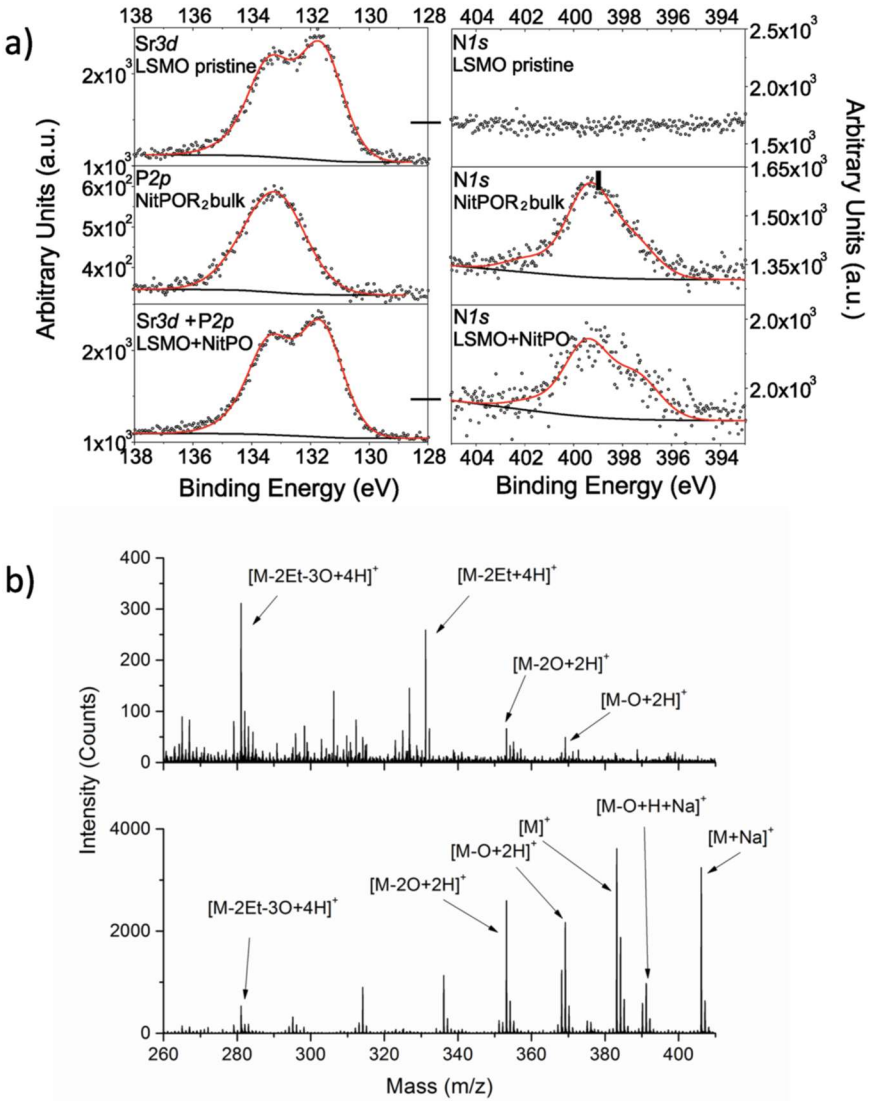

Figure 2. Chemical characterization of the NitPO monolayer assembled on LSMO: a) XPS analysis: XPS spectra in N1s, P2p/Sr3d regions for LSMO pristine (top), bulk $NitPOR_2$ (middle), and NitPO monolayer on LSMO. b) Comparison between ToF-SIMS spectra of a bulk $NitPOR_2$ sample and the NitPO monolayer on LSMO in the region 270–410 *m/z*.

4.2. Electronic Structures and Magnetic Properties

Table 1 summarizes the calculated magnetic moments of the radical and the Mn, La, and Sr atoms of the LSMO surface, in which the moments of LSMO are shown in the first and second columns (see also in the Supporting Information the discussion on the density of states, DOS for the clean LSMO surface). The inspection of the local moment of each Mn atom (not shown in the table) does not reveal any Mn^{3+}–Mn^{4+} charge-ordering effect, as expected due to delocalization effects occurring in a metal. [42]

	MnO_2	LaSrO	Nit-POR_2	NitPO	NitPO/MnO_2	NitPO/LaSrO
Mn(top)	3.759	3.557			3.717	3.611
Mn(mid)	3.317	3.648			3.339	3.611
Mn(bottom)	3.43	3.54			3.452	3.537
La(top)	0.029	0.02			0.029	0.018
La(mid)	0.025	0.026			0.025	0.025
La(bottom)	0.045	0.029			0.046	0.029
Sr(top)	0.008	0.005			0.008	0.003
Sr(mid)	0.007	0.006			0.007	0.005
Sr(bottom)	0.009	0.007			0.009	0.007
N1			0.184	0.182	0.173	0.19
N2			0.175	0.175	0.162	0.18
O1			0.241	0.239	0.221	0.248
O2			0.238	0.239	0.219	0.239
C1			−0.057	−0.057	−0.057	−0.055

Table 1. Selected local magnetic moments, in μ_B, for Mn, La, and Sr (top, mid, bottom) labels the average moment per chemical species located in top, mid, and bottom layer. Columns are relative to the clean surface (first and second column), isolated molecules (third and fourth column), and joint systems (fifth and sixth column).

Thus, no relevant information on the local moment is missing by averaging the magnetic moments per layers, as reported in Table 1. The magnetic moments of the nitronylnitroxide radical are localized on the N-O groups, with a slight amount of negative spin moment on the bridging C atom. Very similar values of magnetic moments are obtained for the $NitPOR_2$ and NitPO molecules; this is expected, since there is no relevant change in the structure, apart from the substitution of CH_2-CH_3 groups by H atoms. Importantly, when anchoring the radical to the LSMO surface, the molecular magnetic character of the NitPO persists. Only a slight reduction of the spin densities for NitPO/MnO_2 can be noticed, and conversely, a slight increase upon the deposition on the LaSrO terminated surface. The changes of the magnetic moments are observed to be even smaller than those of other nitronyl-nitroxide related radicals deposited on gold surface, recently reported. [43]

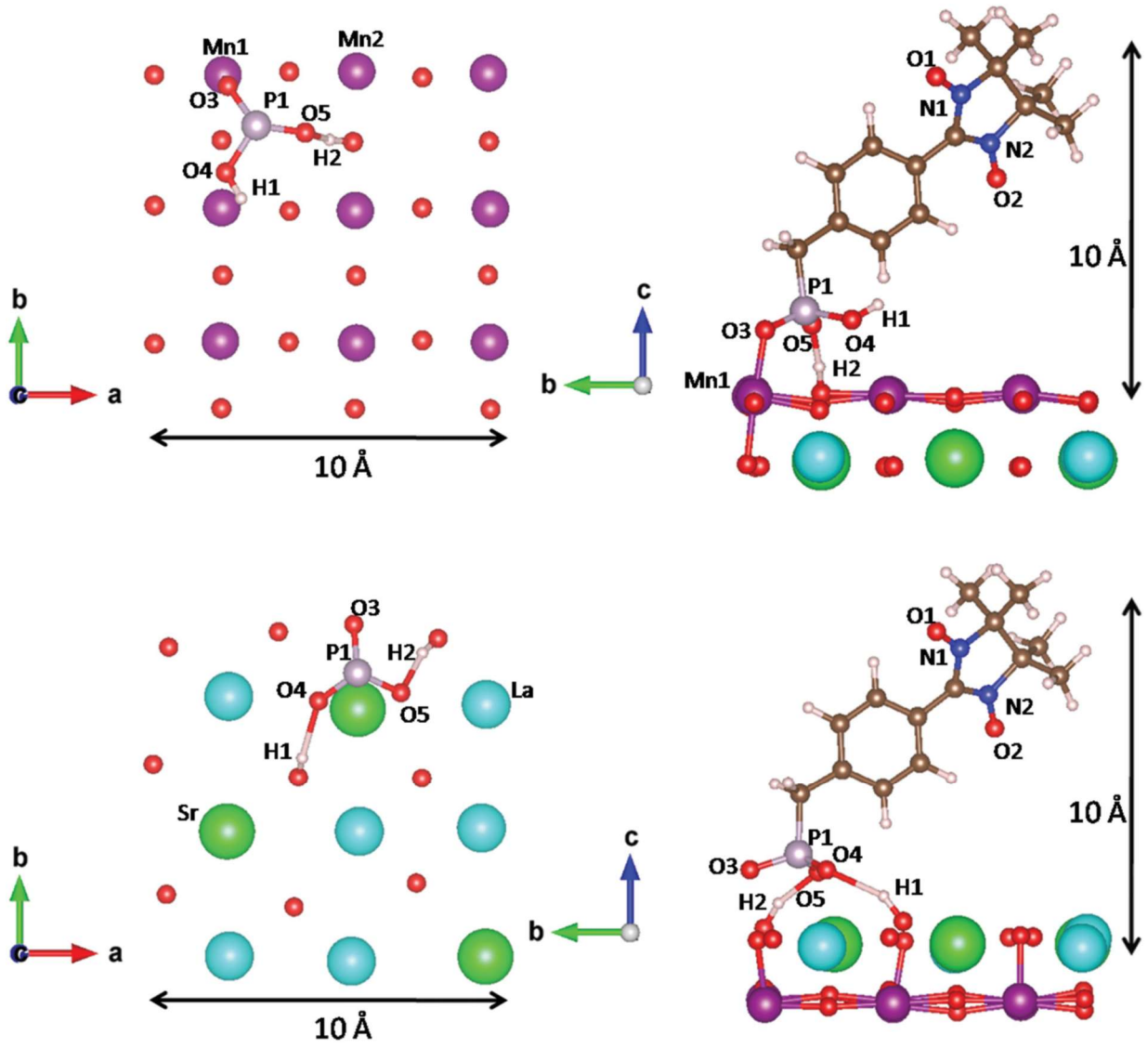

Figure 3. Optimization with MnO_2 (top) and LaSrO (bottom) layer terminations. Top view and side view of the most stable adsorption geometries are shown in the left and right panels respectively. For the sake of clarity, only the phosphonate group of the molecule is displayed in the top views.

It is also worth noting that the oxygen atom O_4 of the molecule shows some tiny induced moment of 0.015 μB (not shown in Table 1) upon adsorption on MnO_2 surface. Being this O atom positioned as apical ligand atom of Mn1 (cfr. Figure 3 a), the induced moment is likely due to the delocalization tail of the Mn magnetic moment. Similarly, the magnetic moments of the LSMO surface after adsorption do not seem to be altered, when compared to those of the clean surface. To summarize, we observe only small changes in the computed moments on both the molecule and substrate due to the adsorption of NitPO on the LSMO surface. The obtained geometry is such that the nitronyl-nitroxide moieties of the molecule are pointing away from the surface (Figure 3), thus making the molecular magnetic moments spatially distant from the surface (indeed, the length of NitPO radical molecule is around 10 Å). It was outlined in previous studies on related surface-radical interfaces [44–47] that such geometry is expected to minimize direct molecule-surface interaction, hence leaving the magnetic molecular orbitals of the radicals unperturbed. This picture is consistent with the spin density plot for NitPO/MnO_2 (see Figure S8a in the Supporting Information), showing extremely weak charge and spin interaction between

substrate and molecule. In this sense, the magnetic behavior of both subsystems is conserved upon adsorption. In order to shed further light on the interaction between the NitPO and the LSMO surface, we focus our attention on the ferromagnetically coupled NitPO/MnO_2 interface, by showing in Figure 4 the density of states of the NitPO molecule after adsorption, together with the atomic projected DOS (PDOS) on the Mn atoms at the surface top layer.

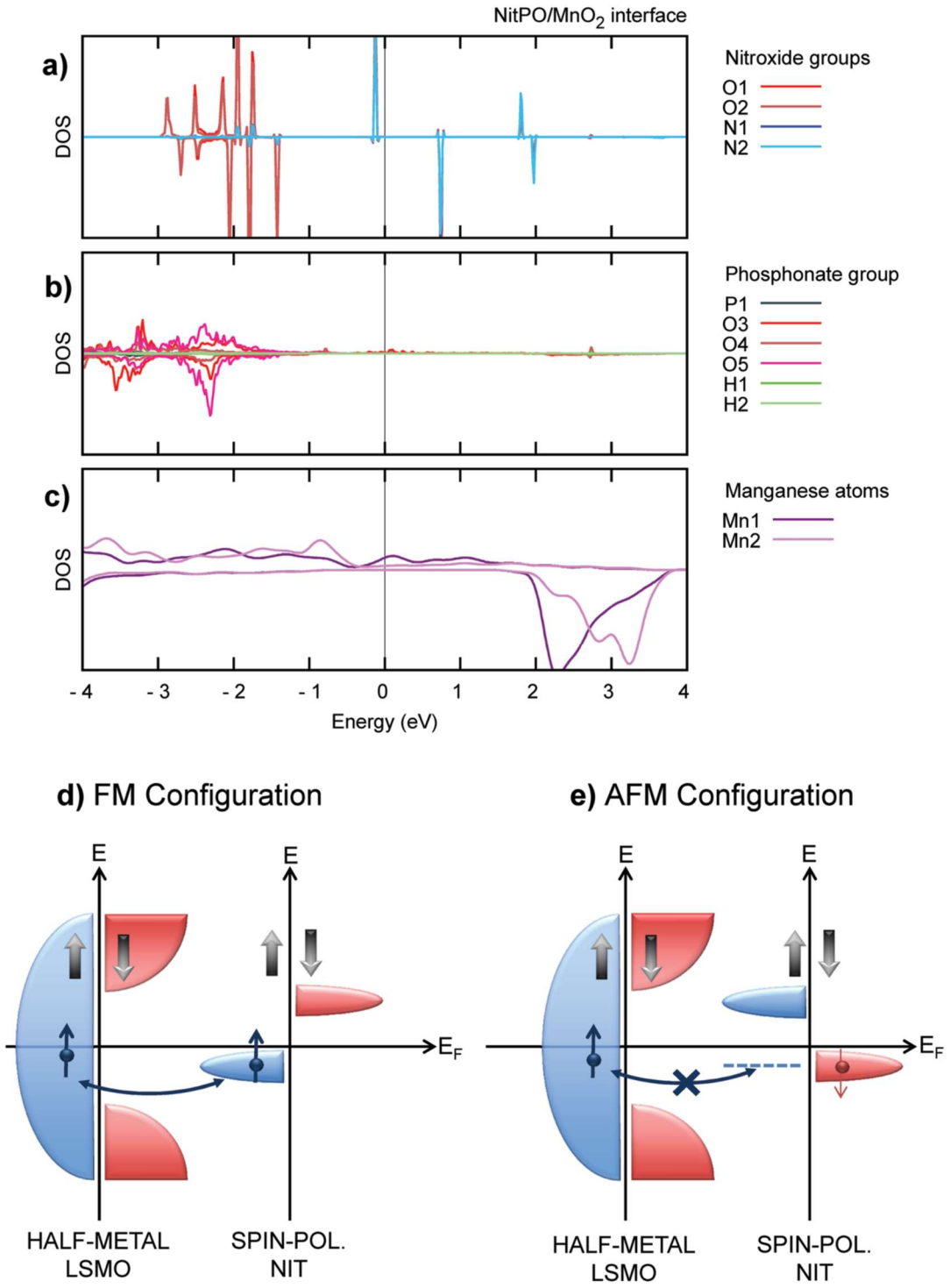

Figure 4. PDOS of the adsorbed molecule (NitPO) in the LSMO/NitPO FM configuration, as projected onto a) nitronlyl nitroxide and b) phosphonate groups, and c) Mn1 and Mn2 atoms at the surface top layer. Schematic spin-resolved band line-up for LSMO (left) and NitPO (right): d) FM configuration and e) AFM configuration.

The persistence of the magnetic character of NitPO is apparent from the PDOS of atomic species carrying the magnetic moments, i.e., the nitroxide groups (similar results are obtained for the molecule deposited on LaSrO-terminated surface). The relative positions of the peaks (especially near the Fermi level) for the NitPO deposited on the surface are not significantly different with respect to those for isolated NitPO (see Figure S6 in the Supporting Information). In the phosphonate group, however, the broadening of the DOS due to adsorption is clearly observed. In fact, as the molecule is anchored to the surface via the phosphonate group, a delocalization of the molecular electronic structure in the energy region below −1 eV can be observed, due to the overlap with the manganese d -band. Focusing now on the surface Mn atoms, an increase in the intensity of PDOS onto the Mn1 atom directly connected to the phosphonate group via O_3 (cfr. Figure 3 a) can be observed at the Fermi level, E_F whereas Mn_2 PDOS is basically unaltered by the adsorption. The DOS of Mn1 resembles those of Mn atoms in deeper layer (see Figure S5 in the Supporting Information), the main difference being the intense peak around −2 eV for the DOS of the Mn's inner layer (attributed to t_{2g} states). As a matter of fact, although Mn1 recovers sixfold octahedral coordination (via the O_3 of the molecule), its structural configuration is more tilted compared to the bulk-like one. As for the band line-up, an important issue is to be noted: the LSMO/NitPO interface shows a spin-filtering effect, arising from (i) the LSMO/NitPO FM coupling, (ii) the energy position of the spin-polarized molecular levels in proximity to the Fermi level, and (iii) the half-metallic nature of LSMO. In fact, as schematically illustrated in Figure 4 d–e, the molecular spin-up HOMO state (the highest occupied molecular orbital) lies very close to the Fermi energy, where LSMO majority electrons can hop; on the other hand, the corresponding spin-down LUMO state (the lowest unoccupied molecular orbital) in the minority spin-channel lies at an energy much higher than E F and within the minority gap of LSMO. As a result, the LSMO/NitPO band line-up is clearly spin-dependent, favoring one spin-channel over the other. For the sake of clarity, we also illustrate the band line-up for the AFM configuration (shown schematically in Figure 4 e and in Figure S7 in the Supporting Information) with HOMO (LUMO) state now parallel to minority (majority) LSMO spins: in this case not only minority spins but also majority spins from LSMO are prevented from hopping on NitPO levels, likely leading to higher resistance.

5. Device Preparation and Characterization

To investigate the effects on spin transport obtained by decorating with a monolayer of organic radicals the interface between the ferromagnetic electrode and the OSC, a NitPO-based spin valve has been realized by using the protocol described above promoting the chemisorption of these stable organic radicals on patterned LSMO spin injecting electrodes deposited on a strontium titanate oxide (STO) substrate. After the deposition of the NitPO, a 150 nm molecular film of Gaq_3 was thermally evaporated on the functionalized surface, and the spin valve was finalized by depositing a cobalt electrode similarly to earlier reports. [48] An additional layer of AlO_x (thickness 2 nm) was interposed between the Gaq_3 and the Co layers to avoid interdiffusion of the metal inside the OSC and possible creation of short-circuits between the two ferromagnetic layers. [12] A device with a vertical geometry was in this way obtained (Figure 1) where the LSMO and Co electrodes are characterized by different values of coercive fi elds in order to observe the spin-valve effect induced by the different orientation of the magnetization of the two electrodes. The temperature dependent transport properties are reported in the Supporting Information. Here, we focus on the magnetic fi eld dependent transport behavior of the device and to its comparison with the ones without the magnetic radical at the interface. In order to characterize the magnetoresistance (MR)

properties of the spin valve, the dependence of the resistance on the external magnetic fi eld applied along the device surface was measured at different temperatures in a range between 2.5 and 300 K (see Figure S7 in the Supporting Information). For each value of the magnetic fi eld, electric transport properties were characterized by measuring in 2-wire mode the current flowing through the device maintaining a fixed potential difference $V_{Co} - V_{LSMO} = 100$ mV between the LSMO and Co electrodes. In this way, being $V_{LSMO} < V_{Co}$, the LSMO electrode acts as a spinpolarized carrier injector and the current flows perpendicularly to the interface between the organic component and the electrodes. Magnetoresistance, defined as $MR = \frac{R(\uparrow\uparrow)-R(\uparrow\downarrow)}{R(\uparrow\uparrow)} \times 100$ where R(↑↑) and R(↑↓) are respectively the resistance values showed by the spin valve when the magnetic moments of Co and LSMO electrodes are parallel and antiparallel, obtained at T = 100 and 3 K, are reported in Figure 5 a,b, respectively, showing values typical for devices without the NitPO layer. [12] Moreover, these devices maintain the inversion of the MR (i.e., R(↑↑) > R(↑↓)) common to Mq_3 (M = Al, Ga) based spin valves with LSMO and Co electrodes [12,36] and explained through a spin-down selective filtering at LSMO/Gaq_3 interface. [14] This indicates that the insertion of paramagnetic molecules NitPO does not induce drastic modifications of the spin injection at the LSMO/Mq_3 interface [14] in reasonable agreement with DFT calculations. The NitPO insertion induces nevertheless a clearly detectable reduction of the magnetoresistance at low temperatures. Figure 5 c reports the dependence of MR as function of T in the so called linearizing plot where the parabolic dependence of MR (T) is clearly revealed by plotting MR 1/2 versus T. As already discussed previously, [12] this parabolic trend is fully described by the spin polarization extracted from the manganite electrode, the most sensitive component to temperature variation. While the standard device (green dots) shows no sizable deviations from this low, a distinct dip of MR 1/2 values is visible below 25 K for NitPO interfaced device (blue dots). Interestingly, the same temperature region is characterized by another deviation from the projected spin valve behavior. Figure 5 d shows the temperature trend of the parallel–antiparallel (low) switching fi eld corresponding to the minimum in the MR curves. This fi eld is typically attributed to the coercive fi eld of the manganite spin polarized electrode, [17] reflecting also possible interfacial modifications. [14] While the coercive fi eld extracted from the longitudinal magnetoresistance of the manganite stripe (see Figure S11 in the Supporting Information) increases monotonically, as expected, with lowering temperature (orange dots in Figure 5 d), an explicit drop of the switching fi eld occurs in the device geometry (in violet) where the current is perpendicular to organic-LSMO interface. While it is not easy to give at this stage a full quantitative description of the observed effects, there is a very good qualitative agreement with DFT results, having the latter revealed a strong spin-up filtering at the LSMO/NitPO interface (see Figure 4). Indeed the introduction of NitPO monolayer includes channels of opposite spin filtering (spin-down filtering at bare interface, see above), reducing thus the overall spin polarization and hence the magnetoresistance. Indeed this takes place at temperatures where the moderate ferromagnetic interaction between LSMO and NitPO is playing a significant role, while at higher temperatures the random magnetic orientation of the molecules with respect to the one of LSMO nullifies this effect.

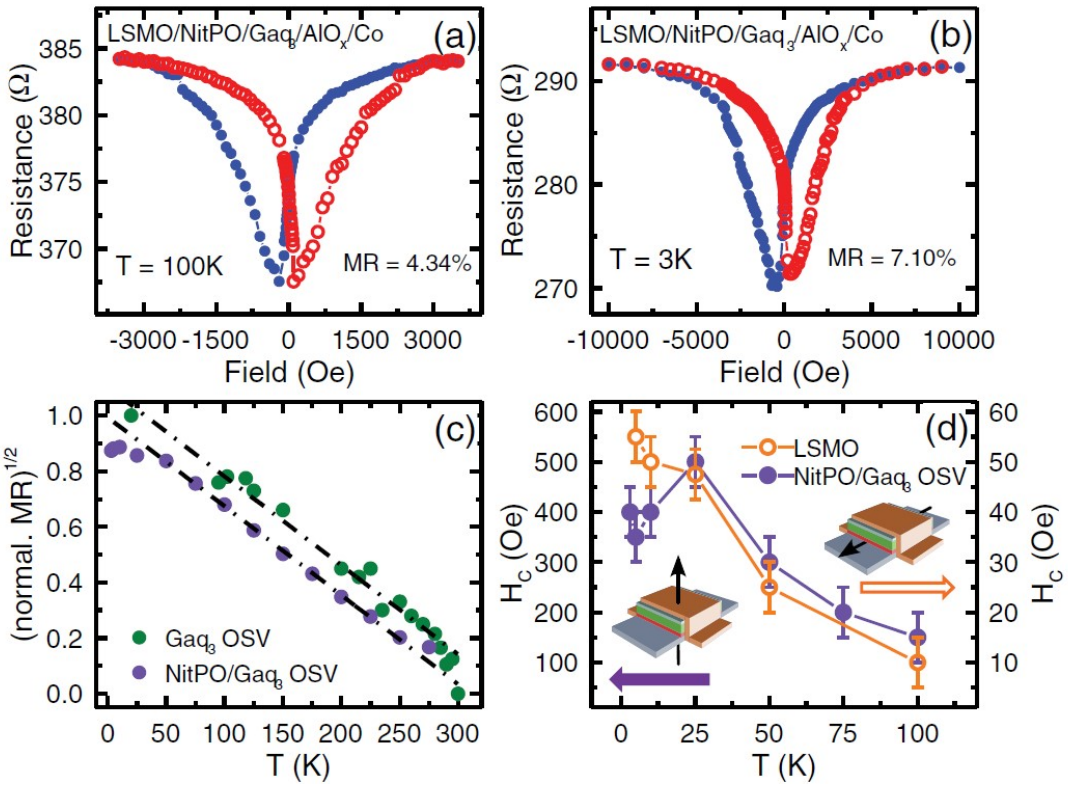

Figure 5. Inverse spin-valve effect detected on NitPO-based device at a) 100 K and b) 3 K; c) linearizing plot for the MR versus temperature for a standard device (no NitPO, green dots [12]) and the NitPO-based device (violet dots). Black lines are guides to the eye. d)Temperature dependence of low switching fi eld (violet dots) corresponding to the minimum of the resistance in MR(T) curves; the orange open dots delineate the bulk coercive field of the manganite stripe extracted from the MR detected in longitudinal configuration.

The exact geometry of spin-up and spin-down filtering channels remains hidden, and will be object of further dedicated research. Indeed, one can model the junction as a series or parallel connection between filtering processes respectively due to LSMO/NitPO/Gaq$_3$ interfaces and [LSMO/NitPO/Gaq$_3$ + LSMO/Gaq$_3$] interface. The former supposes that NitPO is represented by a continuous interfacial layer offering a spin-up spin filtering, and the opposite spin filtering by the Gaq$_3$ is maintained nonetheless the absence of a direct contact between this molecule and manganite. The latter, that looks to us more realistic, relates to a partial coverage of surface by NitPO and describes spin-up channels of LSMO/NitPO/Gaq$_3$ embedded into the spin-down matrix of LSMO/Gaq$_3$. The additional magnetic softening observed at low temperature (the decrease in switching fi elds, see Figure 5 d) though not further investigated in our DFT analysis, can be described by a decrease in coercivity of the modified interface, given the isotropic nature of the radicals magnetically coupled to the LSMO. In any case an electronic (hybridization) origin for this effect seems to be excluded as the latter would have affected the coercivity at higher temperatures.

6. Conclusion

A monolayer of stable organic radicals has been assembled on a LSMO substrate by spontaneous deprotection of the phosphonate group introduced to the nitronyl-nitroxide derivative; grafting has been confirmed by XPS and ToF-SIMS experiments. Though experimental evidence of the persistence of the unpaired spin on the organic molecules are hardly achievable due to the overwhelming magnetism of the substrate, a detailed DFT investigation has provided a clear picture of the adsorption mechanism, evidencing a weak

ferromagnetic interaction between the radical unpaired electron and LSMO (independently of the Mn O or Sr O termination) and a spin-filtering effect, based on the spin-dependent band line-up. When the layer of NitPO is embedded in a vertical device a negative spinvalve effect typical of other OSC based spin-valves is observed, with MR values comparable to the ones observed in similar devices without magnetic molecules. The presence of the NitPO layer, however seems to affect the magnetoresistance at low temperatures when effects due to the magnetic exchange interactions between the radicals and the LSMO layer are foreseen by DFT calculations. Though the mechanism of spin injection in the OSC is still debated and local measurements to avoid the overwhelming contribution of defects and conduction through filament structures are necessary to ascertain the origin of the differences in the field dependence of MR in the device embedding the organic radicals, the persistence of the spin-valve effect is on its own an important result, as scattering induced by the unpaired electron of the radicals was expected. Moreover, comparably high values of MR are observed, although the device preparation differs significantly from the commonly employed ultrahigh vacuum (UHV) procedure; the chemically functionalized LSMO is in fact employed without any further treatment. These results open the perspective of a functionalization of the spin injecting electrode with other types of magnetic molecules exhibiting intrinsic bistability, like single molecule magnets or spin cross-over compounds.

7. Experimental Section

Samples Preparation: Monolayer of NitPO on homogeneous LSMO and patterned LSMO surfaces was prepared in a portable glove-bag by incubating $NitPOR_2$ at 330 K for 20 h in 3×10^{-3} M dichloromethane/ methanol (1:3) solutions of the molecules on 10 nm film of LSMO deposited on STO by spark ablation. [36] Before the incubation, the LSMO was cleaned in acetone and isopropanol for 10 min both in an ultrasonic bath. After incubation, the functionalized surface was rinsed several times with dichloromethane and methanol in order to leave on the surface only the chemisorbed molecules and dried with anhydrous nitrogen gas.

The bulk samples used for XPS and ToF-SIMS experiments as references to be compared with monolayers sample were prepared by drop casting a 2×10^{-3} M solution of $NitPOR_2$ dissolved in methanol and leaving the solvent evaporate under inert atmosphere.

ToF-SIMS Characterization: ToF-SIMS characterization was performed using a TRIFT III time-of-flight secondary ion mass spectrometer (Physical Electronics, Chanhassen, MN, USA) equipped with a gold liquid-metal primary ion source. Positive ion spectra were acquired with a pulsed, bunched 22 keV Au^+ primary ion beam, rasterizing the ion beam over a 10^4 μm^2 sample area. The primary ion dose was kept below 10^{11} ions cm^{-2} to maintain static SIMS conditions. 2 Mass spectra were calibrated to CH_3^+ (m/z 15.023), $C_2H_3^+$ (m/z 27.023), $C_7H_7^+$ (m/z 91.05), and Mn^+ (m/z 54.93), Sr^+ (m/z 87.90), and La^+ (m/z 138.90) (the latter three only for monolayer spectra). For the monolayer sample, mass resolutions were 5760 m/Δm while for bulk ones it was 38500 m/Δm. These variations in Δm/m do not alter significantly our analysis. All the samples were treated under inert atmosphere before the insertion in the UHV chamber.

Electron-Spray Ionization (ESI)-Mass Characterization: ESI mass spectra were recorded infusing the sample solution of 10^{-5} M directly into the ESI chamber by syringe pump. The characterization was performed with a ThermoFisher LCQ-Fleet ion-trap instrument and spectra were recorded by using ESI + techniques. Ion mass/charge (m/z) ratios are reported as values in atomic mass units followed by the intensities relative to the base peak in parentheses.

XPS Characterization: XPS experiments were carried out in a UHV apparatus with a base pressure in the 10^{-10} mbar range. Nonmonochromatized Al Kα radiation was used for XPS measurements (1486.6 eV, 110 W). The detector was a VSW hemispherical analyzer mounting a single-channel detector, the angle between the analyzer axis and the X-ray source was 54.44°. The XPS spectra were measured with a fixed pass energy of 44 eV. The binding energy scale was calibrated setting the C1s signal of the adventitious carbon 284.5 eV. In order to minimize air exposure and atmospheric contamination, samples were mounted on sample holder under dry nitrogen environment in a portable glove bag which was then connected to the fast-entry lock system of the XPS chamber. Spectral analysis consisted in a linear background subtraction and deconvolution using a mixed Gaussian and Lorentzian line-shapes for each spectral component. The stoichiometry of the samples was calculated by peak integration, using sensitivity factors reported for constant band-pass filter machines with similar geometric configuration in the www.uksaf.org database.

Computational and Structural Details: Ab initio calculations have been performed within the DFT framework using the generalized gradient approximation (GGA) functional [49] as implemented in Vienna ab-initio simulation package (VASP). [50] The projected augmented wave (PAW) potentials [51] with a cut-off energy of 500 eV were used. The on-site Coulomb repulsion for the Mn atoms was included using the GGA+*U* approach, as proposed by Dudarev et al. [52] where the Coulomb and exchange parameters U and J were set to be 3 and 0.7 eV, respectively. [42] A 4 × 4 × 1 Monkhorst-Pack grid [53] k-point mesh centered at for the Brillouin zone sampling was used. For the geometry optimization, the ions are relaxed until the forces were smaller than 0.01 eV $Å^{-1}$. The convergence criteria for the electronic self-consistent loop was set to 10^{-5} eV. The dispersion correction in our calculation was included by applying the D2 method of Grimme. [54] The molecular adsorption was modeled by depositing the NitPO radical on the (001)-terminated LSMO surface (see Figure S5c in the Supporting Information). The LSMO surface was modeled with a three layer thick slab, comprising an area of 3 × 3 unit cells, for a total of 135 atoms. As starting geometry, the crystal structure of LSMO grown on top of $SrTiO_3$ substrate, [55] with experimental values of in-plane and out-of-plane lattice constants of a = 3.905 Å and c = 3.850 Å, respectively was considered. A sufficiently thick vacuum layer was included in the slab, resulting in a simulation cell size of 44.650 Å along the z -direction. Moreover, the dipole correction [56] to avoid spurious dipole effects that may arise along the out-of-plane direction was included. Since conflicting information are reported in literature regarding the surface termination of LSMO grown on STO substrate, either showing the presence of MnO_2 termination layer [57,58] or SrO one, [41,59] both terminations are considered in the present study. This choice is consistent with previous experimental characterization of similar LSMO films performed by some of the authors [41] showing both Mn-rich and Sr-rich surface terminations. NitPO/MnO_2 and NitPO/LaSrO notations were used in the text to indicate the NitPO/LSMO adsorbate with the MnO_2 and LaSrO layer terminations, respectively (see Figure S5c in the Supporting Information). Several adsorption sites and molecule orientations were explored, and a total amount of 10 starting models for each termination layer were considered for the geometry optimizations, which were performed by keeping fixed the atomic positions of the bottom layer. Finally, to include the effect of magnetic properties of the NitPO radical on the electronic structure of the system, the geometry optimizations were performed for both FM) and AFM alignments of the magnetic moment of NitPO with respect to those of the LSMO surface, in which the atomic spins are aligned ferromagnetically.

Electric Transport Measurements: Electric transport measurements were carried out with a Keithley 2601a SMU. The instrumentation was interfaced with a PPMS by Quantum Design in order to perform measurements at cryogenics temperatures (down to 2.5 K) and in presence of magnetic fi elds (up to 7 T). Measurements were performed in 2 wire-mode supplying voltages between Co and LSMO

electrodes and measuring the current. For MR measurements a constant voltage $V_{Co} - V_{LSMO} = 100$ mV was employed. Connections to the devices were supplied by gold wires fixed with indium to the samples and to the PPMS sample holders.

Supporting Information

Supporting Information is available from the Wiley Online Library or from the author.

Acknowledgements

The authors are grateful to Prof. Agnese Magnani for assistance in collecting ToF-SIMS data and to Prof. Lorenzo Sorace for assistance in recording EPR spectra. The authors acknowledge the financial contribution of Italian MIUR through the FIRB project RBAP117RWN and of the European Research Council through the Advanced-Grant "MolNanoMaS" (267746).

References

[1] O. Kahn , Molecular Magnetism , Wiley-VCH Verlag GmbH , New York 1993 .

[2] D. Gatteschi , R. Sessoli , J. Villain , Molecular Nanomagnets , Oxford University Press , Oxford 2006 .

[3] R. Sessoli , D. Gatteschi , A. Caneschi , M. A. Novak , Nature 1993 , 365 , 141 .

[4] A. Caneschi , D. Gatteschi , C. Sangregorio , R. Sessoli , L. Sorace , A. Cornia , M. A. Novak , C. Paulsen , W. Wernsdorfer , J. Magn. Magn. Mater. 1999 , 200 , 182 .

[5] M. N. Leuenberger , D. Loss , Nature 2001 , 410 , 789 .

[6] J. R. Friedman , M. P. Sarachik , J. Tejada , R. Ziolo , Phys. Rev. Lett. 1996 , 76 , 3830 .

[7] L. Thomas , F. Lionti , R. Ballou , D. Gatteschi , R. Sessoli , B. Barbara , Nature 1996 , 383 , 145 .

[8] M. Mannini , F. Pineider , C. Danieli , F. Totti , L. Sorace , P. Sainctavit , M.-A. Arrio , E. Otero , L. Joly , J. C. Cezar , A. Cornia , R. Sessoli , Nature 2010 , 468 , 417 .

[9] V. A. Dediu , L. E. Hueso , I. Bergenti , C. Taliani , Nat. Mater. 2009 , 8 , 707 .

[10] T. Shimada , H. Nogawa , T. Noguchi , Y. Furubayashi , Y. Yamamoto , Y. Hirose , T. Hitosugi , T. Hasegawa , Jpn. J. Appl. Phys. 2008 , 47 , 1184 .

[11] X. Z. Wang , X. M. Ding , Z. S. Li , Y. Q. Zhan , I. Bergenti , V. A. Dediu , C. Taliani , Z. T. Xie , B. F. Ding , X. Y. Hou , W. H. Zhang , F. Q. Xu , Appl. Surf. Sci. 2007 , 253 , 9081 .

[12] V. Dediu , L. Hueso , I. Bergenti , A. Riminucci , F. Borgatti , P. Graziosi , C. Newby , F. Casoli , M. De Jong , C. Taliani , Y. Zhan, Phys. Rev. B 2008 , 78 , 115203 .

[13] A. Droghetti , S. Steil , N. Großmann , N. Haag , H. Zhang , M. Willis , W. P. Gillin , A. J. Drew , M. Aeschlimann , S. Sanvito , M. Cinchetti , Phys. Rev. B 2014 , 89 , 094412 .

[14] C. Barraud , P. Seneor , R. Mattana , S. Fusil , K. Bouzehouane , C. Deranlot , P. Graziosi , L. Hueso , I. Bergenti , V. Dediu , F. Petroff , A. Fert , Nat. Phys. 2010 , 6 , 615 .

[15] S. Sanvito , Chem. Soc. Rev. 2011 , 40 , 3336 .

[16] K. V Raman , A. M. Kamerbeek , A. Mukherjee , N. Atodiresei , T. K. Sen , P. Lazi , V. Caciuc , R. Michel , D. Stalke , S. K. Mandal, S. Blügel , M. Münzenberg , J. S. Moodera , Nature 2013 , 493 , 509 .

[17] N. Atodiresei , V. Caciuc , P. Lazi , S. Blügel , Phys. Rev. B 2011 , 84 , 172402 .

[18] Y. Wang , J. G. Che , J. N. Fry , H. P. Cheng , J. Phys. Chem. Lett. 2013 , 4 , 3508 .

[19] M. Callsen , V. Caciuc , N. Kiselev , N. Atodiresei , S. Blügel , Phys. Rev. Lett. 2013 , 111 , 106805 .

[20] A. Scheybal , T. Ramsvik , R. Bertschinger , M. Putero , F. Nolting , T. A. Jung , Chem. Phys. Lett. 2005 , 411 , 214 .

[21] H. Wende , M. Bernien , J. Luo , C. Sorg , N. Ponpandian , J. Kurde , J. Miguel , M. Piantek , X. Xu , P. Eckhold , W. Kuch , K. Baberschke , P. M. Panchmatia , B. Sanyal , P. M. Oppeneer , O. Eriksson , Nat. Mater. 2007 , 6 , 516 .

[22] S. Tatay , C. Barraud , M. Galbiati , P. Seneor , R. Mattana , K. Bouzehouane , C. Deranlot , E. Jacquet , A. Forment-Aliaga , P. Jegou , A. Fert , F. Petroff , ACS Nano 2012 , 6 , 8753 .

[23] J. E. Mcdermott , M. Mcdowell , I. G. Hill , J. Hwang , A. Kahn , S. L. Bernasek , J. Schwartz , J. Phys. Chem. A 2007 , 111 , 12333.

[24] M. Mannini , L. Sorace , L. Gorini , F. M. Piras , A. Caneschi , A. Magnani , S. Menichetti , D. Gatteschi , Langmuir 2007 , 23 , 2389 .

[25] N. Crivillers , M. Mas-Torrent , S. Perruchas , N. Roques , J. Vidal-Gancedo , J. Veciana , C. Rovira , L. Basabe-Desmonts , B. J. Ravoo , M. Crego-Calama , D. N. Reinhoudt , Angew. Chem. Int. Ed. 2007 , 46 , 2215 .

[26] H. Murata , M. Baskett , H. Nishide , P. M. Lahti , Langmuir 2014 , 30 , 4026 .

[27] J. M. Rawson , A. Alberola , A. Whalley , J. Mater. Chem. 2006 , 16 , 2560 .

[28] J. Bosch , E. Molins , C. Miravitlles , F. Palacio , J. Veciana , Mol. Cryst. Liq. Cryst. 1990 , 187 , 67 .

[29] J. H. Osiecki , E. F. Ullman , J. Am. Chem. Soc. 1968 , 90 , 1078 .

[30] I. Žutic´ , J. Fabian , S. Das Sarma , Rev. Mod. Phys. 2004 , 76 , 323 .

[31] B. A. Arbuzov , N. N. Zobova , Synthesis 1982 , 1982 , 433 .

[32] R. S. Loewe , A. Ambroise , K. Muthukumaran , K. Padmaja , A. B. Lysenko , G. Mathur , Q. Li , D. F. Bocian , V. Misra , J. S. Lindsey , J. Org. Chem. 2004 , 69 , 1453 .

[33] L. Gorini , A. Caneschi , S. Menichetti , Synlett 2006 , 2006 , 948 .

[34] T. Toda , E. Mori , K. Murayama , Bull. Chem. Soc. Jpn. 1972 , 45 , 1904 .

[35] A. Ulman , Chem. Rev. 1996 , 96 , 1533 .

[36] P. Graziosi , M. Prezioso , A. Gambardella , C. Kitts , R. K. Rakshit , A. Riminucci , I. Bergenti , F. Borgatti , C. Pernechele , M. Solzi , D. Pullini , D. Busquets-Mataix , V. A. Dediu , Thin Solid Films 2013 , 534 , 83 .

[37] C. Viornery , Y. Chevolot , D. Léonard , B.-O. Aronsson , P. Péchy , H. J. Mathieu , P. Descouts , M. Grätzel , Langmuir 2002 , 18 , 2582 .

[38] C. D. Wagner , A. V. Naumkin , A. Kraut-Vass , J. W. Allison , C. J. Powell , J. R. J. Rumble , NIST Standard Reference Database 20, Version 4.1 .

[39] J. Caro , J. Fraxedas , O. Jürgens , J. J. Santiso , C. Rovira , J. Veciana , A. Figueras , B. J. Caro , Adv. Mater. 1998 , 10 , 608 .

[40] F. Busolo , L. Franco , L. Armelao , M. Maggini , Langmuir 2010 , 26 , 1889 .

[41] L. Poggini , S. Ninova , P. Graziosi , M. Mannini , V. Lanzilotto , B. Cortigiani , L. Malavolti , F. Borgatti , U. Bardi , F. Totti , I. Bergenti , V. A. Dediu , R. Sessoli , J. Phys. Chem. C 2014 , 118 , 13631 .

[42] C. Ma , Z. Yang , S. Picozzi , J. Phys. Condens. Matter 2006 , 18 , 7717 .

[43] G. Rajaraman , A. Caneschi , D. Gatteschi , F. Totti , J. Mater. Chem. 2010 , 20 , 10747 .

[44] A. Robin , L. Marnell , J. Bjork , M. S. Dyer , P. S. Bermudez , S. Haq , S. D. Barrett , M. Persson , A. Minoia , R. Lazzaroni , R. Raval , J. Phys. Chem. C 2009 , 113 , 13223 .

[45] S.-A. Savu , I. Biswas , L. Sorace , M. Mannini , D. Rovai , A. Caneschi , T. Chassé , M. B. Casu , Chemistry 2013 , 19 , 3445 .

[46] S. Abb , S.-A. Savu , A. Caneschi , T. Chassé , M. B. Casu , ACS Appl. Mater. Interfaces 2013 , 5 , 13006 .

[47] R. Kakavandi , S.-A. Savu , A. Caneschi , T. Chassé , M. B. Casu , Chem. Commun. 2013 , 49 , 10103 .

[48] M. Prezioso , A. Riminucci , I. Bergenti , P. Graziosi , D. Brunel , V. A. Dediu , Adv. Mater. 2011 , 23 , 1371 .

[49] J. Perdew , A. Ruzsinszky , G. Csonka , O. Vydrov , G. Scuseria , L. Constantin , X. Zhou , K. Burke , Phys. Rev. Lett. 2008 , 100 , 136406 .

[50] G. Kresse , J. Hafner , Phys. Rev. B 1993 , 47 , 558 .

[51] P. E. Blöchl , Phys. Rev. B 1994 , 50 , 17953 .

[52] S. L. Dudarev , G. A. Botton , S. Y. Savrasov , C. J. Humphreys , A. P. Sutton , Phys. Rev. B 1998 , 57 , 1505 .

[53] H. J. Monkhorst , J. D. Pack , Phys. Rev. B 1976 , 13 , 5188 .

[54] S. Grimme , J. Comput. Chem. 2006 , 27 , 1787 .

[55] F. Tsui , M. C. Smoak , T. K. Nath , C. B. Eom , Appl. Phys. Lett. 2000 , 76 , 2421 .

[56] J. Neugebauer , M. Scheffl er , Phys. Rev. B 1992 , 46 , 16067 .

[57] M. Izumi , Y. Konishi , T. Nishihara , S. Hayashi , M. Shinohara , M. Kawasaki , Y. Tokura , Appl. Phys. Lett. 1998 , 73 , 2497 .

[58] M. Yoshimoto , H. Maruta , T. Ohnishi , K. Sasaki , H. Koinuma , Appl. Phys. Lett. 1998 , 187 , 150 .

[59] R. Bertacco , J. P. Contour , A. Barthélemy , J. Olivier , Surf. Sci. 2002 , 511 , 366 .